Bubbles in Flow Streams and Porous Media

J. A. Almonacid [1], A. K. Aydin [2], J. A. Roberts [3], and M. D. Shirley [3]†

[1] *Simon Fraser University, Burnaby, BC, Canada*
[2] *University of Maryland Baltimore County, Maryland, USA*
[3] *University of Oxford, Oxford, UK*

(*Communicated to* MIIR *on 21 February 2024*)

Study Group: MPI 39, NJIT, June 12–16 2023
Communicated by: Linda Cummings
Industrial Partner: W. L. Gore & Associates, Inc.
Presenter: V. Venkateshwaran
Team Members: J. A. Almonacid, British Columbia; A. K. Aydin, Maryland; S. Bohun, Ontario; I. Erazo, Louisiana; H. Fattahpour, Georgia; J.A. Roberts, Oxford; D. Rumschitzki, New York; P. Sanaei, Georgia; M.D. Shirley, Oxford
Industrial Sector: Chemical

Key Words: Electrochemical Reactions, Fluid Dynamics, Bubbles

MSC2020 Codes: 76-10, 76S05, 76T10

Summary

This study explores the behaviour of an electro-chemical device for producing gases such as hydrogen and oxygen. The device consists of two channels of flowing fluid, separated by a porous membrane, with the surface of the membrane coated to act as electrodes of opposite charge. The processes involved in gas production include bubble nucleation, growth, detachment, and potential transport through the porous material, and electro-chemical reactions. These are strongly coupled since the presence of bubbles on the surface of the electrode alters the surface area available for reaction, and the distribution of bubbles in the channel can affect the fluid flow. In this report, two simplified models are developed to understand the behavior of elements of this process. The first model considers the effect of bubbles coating the surface of the electrode on the electrical resistance of the entire system, while the second model focuses on predicting the spatial distribution of disolved gas and bubbles within a single channel.

† Corresponding Author: matthew.shirley@maths.ox.ac.uk

1 Introduction

Gas-liquid interactions within porous materials play a crucial role in various chemical and electrochemical reaction systems involving multiple phases. This type of system involves fluid streams that contain dissolved gases and/or gas bubbles flowing along a flat sheet of porous material. It is important to note that the porous material, a thin composite layer with varying surface energies, is typically saturated with the fluid stream. Often, chemical or electrochemical reactions with fluid reactants take place on the solid surface. As such, the more surface is wetted, the more reaction can proceed, i.e., it is desirable to completely wet the porous material with the liquid. The setup is shown in Figure 1.

In order to optimize processes and designs, it is important to understand the complex dynamics of bubble interactions and dissolved gases within porous materials. In this system, introduced by W. L. Gore & Associates, each side of a vertical porous medium contains an electrode and is exposed to water flowing vertically, possibly at different flow rates, in an enclosed chamber. A current is applied across these electrodes to electrolyze water and thus produce hydrogen gas in one chamber and oxygen gas in the other. The gases can both nucleate bubbles on the electrode surfaces that can grow and detach, as well as dissolve and diffuse into the flowing liquids. An overpressure on the hydrogen side can cause hydrogen bubbles to transport through the porous material to the oxygen-rich side, thereby reducing system efficiency. When bubbles detach, they are transported into and with the flowing liquid, with the potential to grow, shrink, and/or interact (e.g., combine with) other bubbles in time, and eventually leave through the top of the chamber. Bubbles can also nucleate homogeneously in response to local liquid supersaturation. There may also be ions present. Clearly, this is a complex system. In this study, we define several simplified problems that tackle portions of this overall problem. Although during the MPI week, a few of these partial problems have been studied, longer and more intensive research can lead to a deeper understanding of this device and allow for its optimization.

The gas bubbles within each fluid stream can exhibit a wide size distribution and interact with the surface of the porous material through collision, migration, fragmentation, merging, growth, and shrinking mechanisms. Bubble nucleation primarily takes place at the electrode surface, but a region in each liquid called its nucleation zone, which may be different in the two liquid regions, can have local gas supersaturation that can result in some homogeneous nucleation. The gas bubbles and their dynamics can reduce the surface area of the porous material in contact with the liquid phase and, as mentioned, the efficiency-reducing process of bubble migration across the porous material.

In the spirit of studying gas-liquid interaction phenomena within porous materials, extensive research has been conducted to understand their behavior and effects. Previous analyses have focused on investigating bubble dynamics, including collision, migration, fragmentation, merging, growth, and shrinking mechanisms. These studies have explored the influence of various factors, such as pore size distribution, surface energy distribution, curvatures within the pore space, and bubble behavior. Additionally, research has examined the effects of supersaturation and bubble nucleation, as well as the impact of different pressure conditions on bubble migration and distribution. Some studies have also investigated the behavior of bubbles in multi-layered porous materials with varying

properties. Overall, these research efforts have contributed to a better understanding of bubble dynamics and their implications for chemical and electrochemical reactions within porous materials. However, there is still a need for further investigation, and Gore would like to both use existing knowledge and develop new accurate models to understand and optimize their device, including maximizing the bubble-free electrolysis area on the electrode surface and reducing hydrogen transport through the porous material.

In [SDD15], the authors develop a model for electrochemically generated bubbly flow between two vertical electrodes using a mixture model [IH10]. Several assumptions are made about the bubbles, such as neglecting the phenomena of bubble deformation, internal circulation, adherence to the walls, and bubble coalescence and break-off. Motivated by this work, the authors in [RH23a] developed an analytical model for gas fraction profiles near gas-evolving electrodes under a series of stringent assumptions. Nevertheless, they observe the development of a plume of bubbly flow, similar to the temperature profile in the Prandtl boundary layer problem. Some re-entrant flow is also possible.

To address these challenges, this study aims to develop several simplified models that provide insight into the behavior of bubbles in flowing liquids, dissolved gases, and chemical/electrochemical reactions on an electrode surface. These models will partially address key questions regarding the influence of porous material properties, such as pore size distribution, surface energy distribution, and curvatures within the pore space, on the steady-state gas volume fraction within the material.

The remaining report is structured as follows: In §2, we model the electrical behaviour of the separator using an equivalent circuit model. In §3, we consider an alternative model based on transport equations for dissolved gas and bubbles within a single channel of the device. We conclude the report in §4 and discuss other avenues for investigation.

2 A model for the effect of bubbles on electrical resistance

2.1 Flow in the Channel

In this section, we present a model for the flow in the two channels on either side of the porous media.

We assume that these channels are long and thin, *i.e.*, $H, D \ll L$. We conduct our analysis by considering the right hand channel in Figure 2. We assume Stokes flow in the channel and so our governing equations are

$$\nabla \cdot u = 0, \tag{2.1a}$$

$$\nabla p = \mu \nabla^2 u, \tag{2.1b}$$

where u and v are the horizontal and vertical components of the fluid velocity, respectively, p is the pressure, and μ is the viscosity. We assume no-slip boundary conditions on both walls of the channel, a fluid pressure at the bottom of the channel, and 0 pressure at the top. This is given by

$$u(D, y) = \mathbf{0}, \;\; u(D + H, y) = \mathbf{0}, \tag{2.2a}$$

$$p(x, y = 0) = p_{\text{inlet}}, \;\; p(x, y = L) = 0. \tag{2.2b}$$

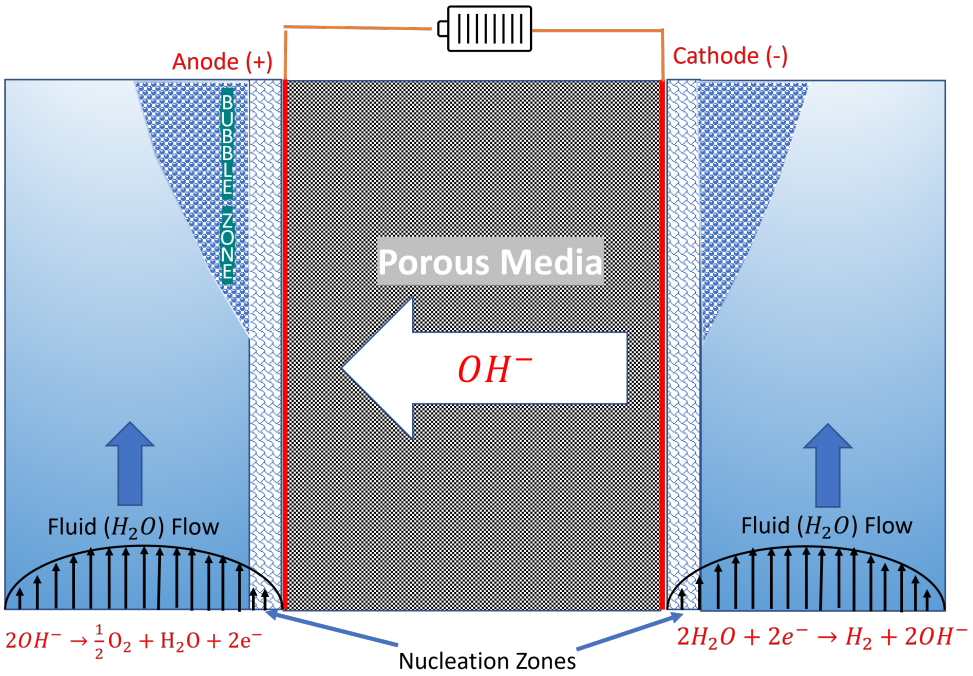

Figure 1. Two channels with fluid flow are connected by a porous membrane with electrodes at both ends. Generated gas over the electrodes nucleates bubbles within nucleation zones. The detached bubbles flow within the bubble zones.

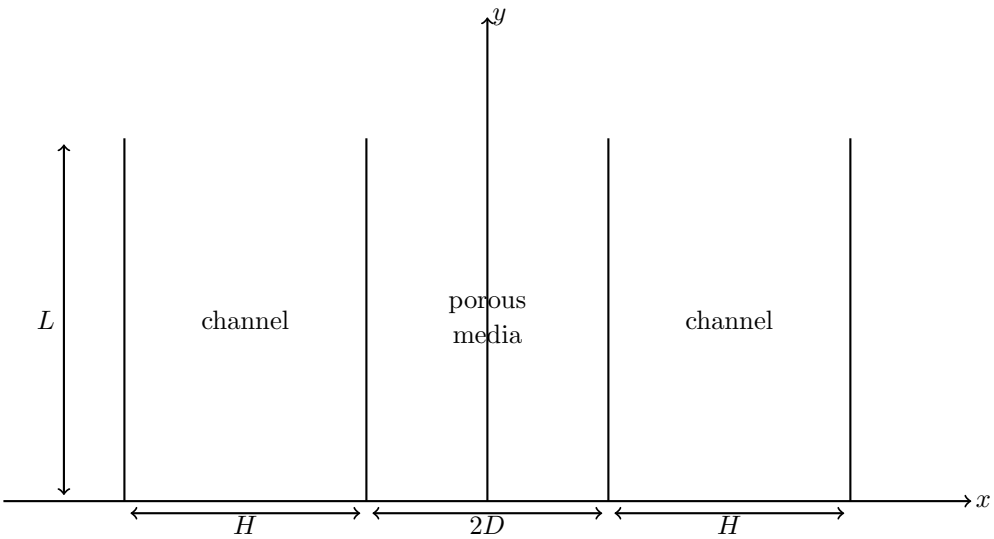

Figure 2. Each channel is assumed to be long and thin, with length and thickness denoted L, and H respectively. The thickness of porous membrane from the center line to each electrode is denoted as D.

We nondimensionalise (2.1) and (2.2) using

$$p = p_{\text{inlet}}\hat{p}, \tag{2.3a}$$

$$u = \frac{p_{\text{inlet}} L\epsilon^2}{\mu}\hat{u}, \tag{2.3b}$$

where $\epsilon = D/L \ll 1$ and hats refer to dimensionless variables. This means equations (2.1) become

$$\frac{1}{\epsilon^2}\frac{\partial p}{\partial x} = \frac{\partial^2 u}{\partial x^2} + \epsilon^2\frac{\partial^2 u}{\partial y^2}, \tag{2.4a}$$

$$\frac{\partial p}{\partial y} = \frac{\partial^2 v}{\partial x^2} + \epsilon^2\frac{\partial^2 u}{\partial y^2}, \tag{2.4b}$$

$$\frac{\partial u}{\partial x} + \frac{\partial v}{\partial x} = 0, \tag{2.4c}$$

with dimensionless boundary conditions

$$u(1+\delta, y) = u(1, y) = 0, \tag{2.5a}$$

$$p(x, y = 0) = 1,\ p(x, y = 1) = 0, \tag{2.5b}$$

where $\delta = H/D$. At leading order, assuming $\epsilon \ll 1$, we therefore have

$$\frac{\partial p}{\partial x} = 0, \tag{2.6a}$$

$$\frac{\partial p}{\partial y} = \frac{\partial^2 v}{\partial x^2}, \tag{2.6b}$$

which we solve subject to (2.5) to give the solution

$$P = 1 - y, \tag{2.7a}$$

$$u = 0, \tag{2.7b}$$

$$v = -\frac{1}{2}\left[x^2 - (2+\delta)x + 1 + \delta\right]. \tag{2.7c}$$

The vertical fluid velocity profile for $\delta = 2$ is shown in figure 3, where we recover the standard Stokes flow result. We can use the results (2.7) to show that the total shear stress in the fluid is given by

$$\tau = \frac{\partial u}{\partial x}(1, y) = \frac{\delta}{2}. \tag{2.8}$$

It is this shear stress (at the boundary between the channel and the wall) that determines whether bubbles detach from the wall. In the next section, we will consider the resistance provided to the system due to the presence of these bubbles.

2.2 A Resistance Model for Bubbles in the Channel

In this section, we use the results of Section 2.1 to inform a model for resistance. During the process, bubbles form along the wall of the fluid channel, creating resistance to the flow of ions. This leads us to model the setup shown in figure 1 as a simple circuit, shown in figure 4, where R_L and R_R are the resistances in the circuit caused by the presence

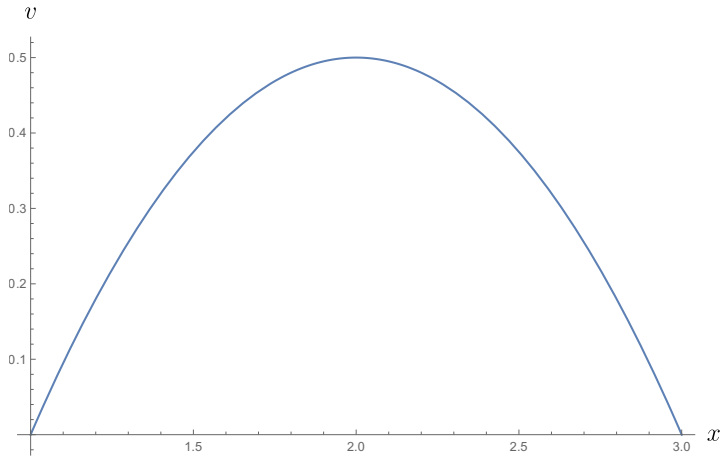

Figure 3. The Stokes flow fluid velocity profile in the narrow channel for $\delta = 2$.

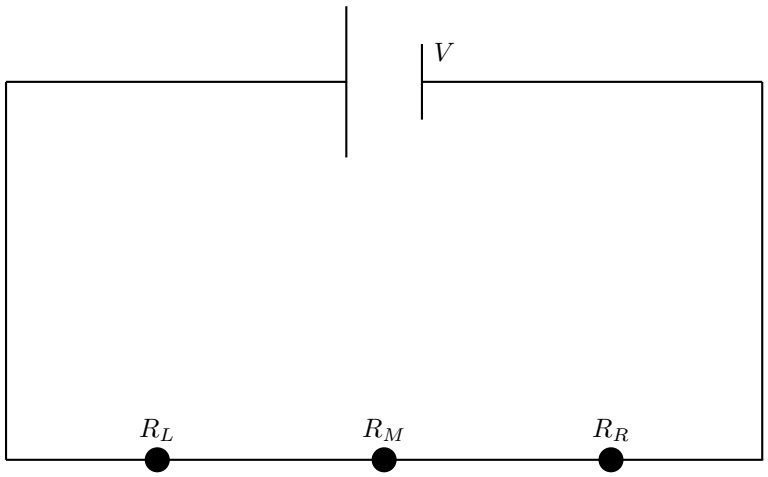

Figure 4. Simple circuit diagram for the formulation of the resistance model.

of bubbles on the left and right inner channel walls, and R_M is the resistance caused by the porous media in between.

From the standard circuit equations, we have that

$$V = IR_t, \tag{2.9a}$$

$$R_t = R_L + R_w + R_R, \tag{2.9b}$$

where V is the voltage of the system, I is the current, and R_t is the total resistance. We assume the voltage is known, and therefore the current is given by (2.9). We then use the standard Tafel equation [PNBT07], namely

$$\frac{I}{nF} = kC \exp\left(\pm \alpha F \frac{V}{RT}\right), \tag{2.10}$$

where n is the number of electrons exchanged, k is the rate constant for the electrode

reaction, F is the Faraday constant, C is the species concentration at the electrode surface, R is the universal gas constant, and α is the charge transfer coefficient. Equation (2.10) gives the value of C, given the current, I. We note the resistances R_L and R_R in the circuit are functions of the bubble density along the channel walls, where the bubble density and volume are given by

$$\rho_b = \frac{CM_m}{\rho_g V_b}, \tag{2.11a}$$

$$V_b = \frac{4}{3}\pi r^3 - \frac{\pi}{3} r^3 (1-\cos\theta)^2(2+\cos\theta), \tag{2.11b}$$

respectively, where M_m is the molar mass of the dissolved gas, ρ_g is the density of the gas, r is the radius of a bubble, assumed to be spherical for now, and θ is the contact angle of the bubbles. From the Young-Laplace equation [SS21] we can relate the pressure difference inside and outside a bubble to the surface tension and contact angle, *i.e.*

$$\Delta P = \frac{2\gamma}{r}, \tag{2.12}$$

where γ is the surface tension, and the pressure inside the bubble is assumed to be 0 so the pressure difference ΔP is given by (2.7a).

Now, we assume the increase in volume of a bubble is driven by the difference in density of gas inside and outside the bubble. When the bubble density is below some critical density, ρ_c, the growth is proportional to $t^{1/2}$, where t is time elapsed, and when the bubble density is above this critical value, its growth is proportional to $t^{1/3}$. We therefore have the equation

$$\frac{\mathrm{d}V_b}{\mathrm{d}t} = \begin{cases} \alpha_1(\rho_b - \rho_c)t^{\frac{1}{2}} + \beta, & \rho_b < \rho_c, \\ \alpha_2(\rho_b - \rho_c)t^{\frac{1}{3}} + \beta, & \rho_b > \rho_c, \end{cases} \tag{2.13}$$

where α_1, α_2 and β are constants. The last equation we need is for how the resistance due to the presence of bubbles (R_R or R_L) evolves with time. We assume that the change in resistance is proportional to the bubble density, *i.e.*,

$$\frac{\mathrm{d}R_R}{\mathrm{d}t} = \alpha_3 \rho_b. \tag{2.14}$$

We nondimensionalize our Eqs. (2.9)-(2.14) and are then left with a system we can solve for the evolution of volume of bubbles and resistance due to these bubbles with time. We assume the initial resistance is 0 and solve for different initial bubble volumes, with the initial results shown in figures 5 and 6. We see the resistance due to the presence of bubbles increasing as the volume of bubbles increases.

We acknowledge that these are very preliminary results to our very simple model, and many parameters have been chosen somewhat arbitrarily. Further analysis and investigation would be needed to fully capture the behaviour of the system.

3 Gas transport model

In order to better understand the distribution of the gaseous products within the channels of the device, both as dissolved species and as bubbles, we now develop a simple model

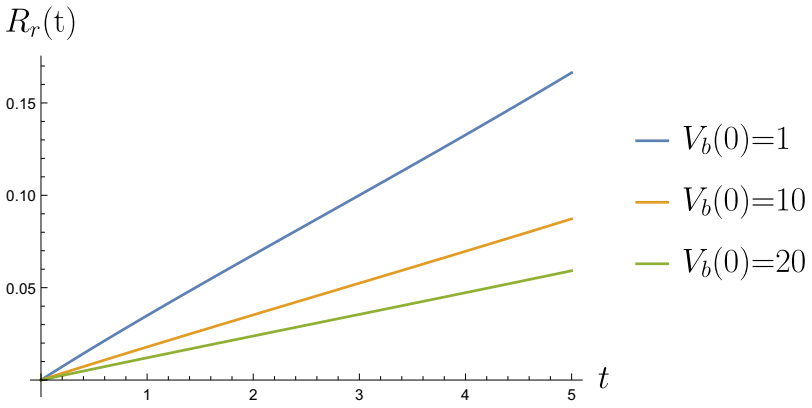

Figure 5. Dimensionless bubble volume against time.

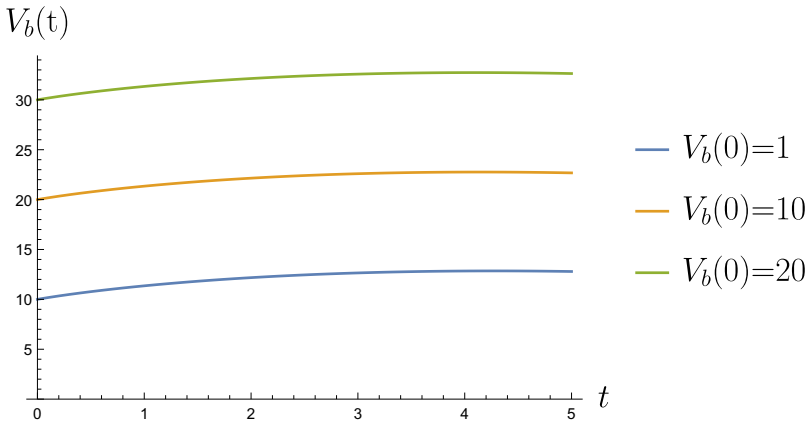

Figure 6. Dimensionless resistance against time.

for a single channel, with the effect of the separator approximated through boundary conditions.

3.1 Model formulation

We now consider a two-dimensional channel of width a, and height h, introducing a Cartesian coordinate system (x, z), such that the channel occupies the region $0 < x < a$, $0 < z < h$. We assume that the separator is positioned at $x = 0$. We assume that other channel has identical dimensions and that the flow through each channel is driven by the same pressure difference. We also assume that the amount of water removed at the cathode by the reaction

$$2\,H_2O + 2\,e^- \longrightarrow H_2 + 2\,OH^- \tag{3.1}$$

and created at the anode by the reaction

$$2\,OH^- \longrightarrow \frac{1}{2}O_2 + H_2O + 2\,e^- \tag{3.2}$$

is negligible. We also assume that the separator is sufficiently rigid and the pore size is small enough for a no-slip condition to be appropriate. Then, assuming the flow to be fully developed and that it is not altered by the presence of bubbles, the fluid velocity, $\mathbf{u}(x,z) = (u(x,z), w(x,z))$, is given by

$$u(x,z) = 0, \qquad w(x,z) = \frac{\Delta p}{2h\mu_0} x(a-x), \tag{3.3}$$

where $\Delta p = p_{in} - p_{out}$ [Pa] is the pressure difference between the inlet and outlet and μ_0 [Pa s] is the viscosity of water.

Note that the no-slip condition on the porous separator may not be appropriate, and a Beavers-Joseph slip condition may be a more realistic choice [JM00]. In such a case, it would be necessary to also consider a vertical flow within the separator itself. The assumption that the flow is unaffected by the bubbles is also unphysical when the bubbles occupy a significant portion of the volume fraction in the fluid. However, considering this effect requires a multiphase flow model, which greatly increases the complexity of the model (for example, see [RH23b]).

We will assume that the dissolved gas, with concentration $c_d(x,z,t)$, is transported by both advection and Fickian diffusion. Consequently, conservation of dissolved gas in the fluid is given by

$$\frac{\partial c_d}{\partial t} + u \cdot \nabla c_d = \nabla \cdot (D \nabla c_d), \tag{3.4}$$

where D is the diffusion coefficient for the dissolved gas [$\mathrm{m}^2\,\mathrm{s}^{-1}$].

In order to consider the simplest possible problem, we will assume that bubbles may only form on the electrode at $x = 0$, and all have the same radius R_b. We assume that the velocity of the bubbles is $\boldsymbol{u}_b = (u_b, w_b)$, are given by the Hadamard–Rybczynski theory for bubble motion, and so is given by

$$u_b(x,z,t) = \frac{2}{3} \frac{R_b^2 \rho_0}{\mu_0} w \frac{\partial w}{\partial x} \frac{\mu_0 - \mu_b}{2\mu_0 + 3\mu_b}, \tag{3.5}$$

$$w_b(x,z,t) = \frac{2}{3} \frac{R_b^2 (\rho_0 - \rho_b)}{\mu_0} g \frac{\mu_0 - \mu_b}{2\mu_0 + 3\mu_b}, \tag{3.6}$$

where ρ_b and μ_b are the density and viscosity of the gas respectively. The horizontal velocity comes from the difference in inertial forces acting on opposite sides of the bubble, while the vertical velocity is due to buoyancy. Given these expressions, we have that conservation of mass of bubbles becomes

$$\frac{\partial c_b}{\partial t} + u_b \cdot \nabla c_b = 0, \tag{3.7}$$

where $c_b(x,z,t)$ [$\mathrm{mol}\,\mathrm{m}^{-3}$], is the concentration of bubbles.

We assume that gas is being created at the electrode surface at rate equal to $q_t f(c_b)$, where q_t is the rate of production of gas using the full electrode surface area, given by the Tafel equation [PNBT07], and assumed to be constant, while $f(c_b)$ is a function accounting for the decrease in reaction rate as the presence of bubbles reduces the available surface area for reaction. Since the Tafel equation assumes the rate of reaction is linearly

proportional to the available surface area, we assume f has the form

$$f(c_b) = 1 - \frac{c_b}{c_{b,\max}}, \tag{3.8}$$

where $c_{b,\max}$ [mol m^{-3}] is the concentration at which the surface of the electrode becomes fully covered.

In the real device bubbles will form at a nucleation site on the surface of the electrode, once the concentration of dissolved gas exceeds a saturation amount $c_{d,\text{sat}}$. The bubble will then grow until it reaches a critical radius where it becomes energetically favourable to detach from the wall. We would like to approximate this process by assuming that bubbles instantaneously form at a rate q_s which is zero for $c_d < c_{d,\text{sat}}$ at the electrode and equal to a positive constant for $c_d > c_{d,\text{sat}}$. To allow the numerical results to converge, in practice we must approximate this behaviour using a tanh function,

$$q_s(c_d) = \mathcal{R}_s\left(1 + \tanh\left(\beta\left(c_d - c_{d,\text{sat}}\right)\right)\right), \tag{3.9}$$

where $\mathcal{R}_s$ [mol s^{-1} m^{-2}] is the rate at which bubbles are forming, then detaching from the electrode, and β [m^3 mol^{-1}] is a parameter controlling the slope of this approximate step function.

By considering conservation of gas close to the electrode, we obtain two boundary conditions for the flux of dissolved gas and bubbles into the flow

$$-D\frac{\partial c_d}{\partial x} = f(c_b)\left(q_t - q_s(c_d)\right), \tag{3.10}$$

$$u_b c_b = f(c_b)\, q_s(c_d). \tag{3.11}$$

Since the horizontal bubble velocity (3.5) is proportional to the vertical fluid velocity, it will be zero at $x = 0$ and $x = a$. This implies that bubbles created at $x = 0$, will never move horizontally. Since, we wish for bubbles to be able to enter the channel in our model, we therefore assume that the bubbles are released one bubble diameter, $2R_b$, away from the surface of the electrode, meaning that the boundary conditions hold at $x = 2R_b$, and the governing Eqs. (3.4), (3.7) hold in $2R_b < x < 1 - 2R_b$, $0 < z < h$.

We assume that there is no dissolved gas or bubbles in the incoming fluid to the channel,

$$c_b = 0, \quad c_d = 0, \quad \text{at } z = 0. \tag{3.12}$$

At the outlet of the channel we impose zero diffusive flux of dissolved gas,

$$\frac{\partial c_d}{\partial z} = 0, \quad \text{at } z = h, \tag{3.13}$$

so that the dissolved gas is simply advected out with the flow. This is the standard choice of a passive boundary condition for an outlet in advection-diffusion problems, as it has little affect upon the upstream behaviour.

On the wall of the channel opposite the separator, at $x = a$, we impose no flux of dissolved gas. Analysis of the characteristics of (3.7) (see §3.5) reveals that we must also impose the concentration of bubbles on this boundary, which we take to be zero, giving

$$c_b = 0, \quad \frac{\partial c_d}{\partial x} = 0, \quad \text{at } x = a - 2R_b. \tag{3.14}$$

Parameter	Symbol	Value	Unit
Dynamic viscosity water	μ_0	1×10^{-3}	$\mathrm{kg\,m^{-1}\,s^{-1}}$
Density water	ρ_0	1×10^{3}	$\mathrm{kg\,m^{-3}}$
Viscosity Hydrogen gas (27 °C, Sutherland law)	μ_b	9.03×10^{-6}	$\mathrm{kg\,m^{-1}\,s^{-1}}$
Diffusion coefficient dissolved Hydrogen (25 °C)	D	5.11×10^{-9}	$\mathrm{m^2\,s^{-1}}$
Width of channel	a	1×10^{-4}	m
Height of device	b	1	m
Saturation concentration for H^2	$c_{d,sat}$	7.9×10^{-4}	$\mathrm{mol\,L^{-1}}$
Pressure gradient	Δp	2500	Pa
Rate of generation dissolved gas	q_t	1×10^{-6}	$\mathrm{mol\,L^{-1}\,s^{-1}}$
Rate of generation bubbles	$\mathcal{R}_s$	1×10^{-10}	$\mathrm{mol\,s^{-2}\,m^{-2}}$
Bubble radius	R_b	1×10^{-6}	m

Table 1. Values of dimensional parameters in the model.

The boundary conditions on the channel wall, (3.14) become

$$\frac{\partial c_d}{\partial x} = 0, \quad c_b = 0, \qquad \text{at } x = 1 - 2\epsilon. \tag{3.15}$$

Appropriate physical parameter values, based on the best estimate that could be found at the study group are given in Table 1, although we expect there to be a large variation across all possible devices.

3.2 Non-dimensionalisation

We now non-dimensionalise the problem as follows,

$$\begin{aligned} x = a\hat{x}, \quad z = h\hat{z}, \\ c_b = c_{b,\max}\hat{c}_b, \quad c_d = c_{d,\mathrm{sat}}\hat{c}_d, \\ w = [w]\hat{w} = \frac{a^2\Delta p}{2h\mu}\hat{w}, \quad q_s = \mathcal{R}_s\hat{q}_s, \end{aligned} \tag{3.16}$$

where hats are used to denote dimensionless variables. Then, assuming the concentrations of the dissolved gas and bubbles to be steady, substituting the scalings (3.16) into the governing Eqs. (3.4)–(3.7), and dropping the hat notation, gives that

$$\delta^2 Pe\, w\frac{\partial c_d}{\partial z} = \frac{\partial^2 c_d}{\partial^2 x^2} + \delta^2\frac{\partial^2 c_d}{\partial z^2}, \tag{3.17}$$

$$Fr^2\, w\frac{\partial w}{\partial x}\frac{\partial c_b}{\partial x} + \delta^2\left(1 - \frac{\rho_b}{\rho_0}\right)\left(1 + \frac{2\mu_b/\mu_0}{1 - \mu_b/\mu_0}\right)\frac{\partial c_b}{\partial z} = 0, \tag{3.18}$$

for $2\epsilon < x < 1 - 2\epsilon$, $0 < z < 1$, where

$$w = x(1 - x). \tag{3.19}$$

This has introduced the following dimensionless parameters into our model,

$$\epsilon = \frac{R_b}{a}, \quad \delta = \frac{a}{h}, \quad Pe = \frac{[w]h}{D}, \quad Fr = \frac{[w]}{\sqrt{gh}}, \quad \frac{\rho_b}{\rho_0}, \quad \frac{\mu_0}{\mu_b}, \tag{3.20}$$

which are the ratio of bubble radius to channel width, ratio channel width to channel height, the Péclet number, the Froude number, and the ratios of gas to liquid density and

viscosity, respectively. The Péclet number is the ratio of the rates of advective transport of the dissolved gas to diffusive transport, while the Froude number is the ratio of inertial forces due to the flow versus gravitational forces acting on the bubbles.

We also nondimensionalise the boundary conditions using (3.16). The conditions at the inlet, (3.12), become

$$c_b = 0, \quad c_d = 0, \quad \text{at } z = 0. \tag{3.21}$$

The boundary condition at the outlet, (3.13), becomes

$$\frac{\partial c_d}{\partial z}, \quad \text{at } z = 1. \tag{3.22}$$

The boundary conditions at the electrode become

$$-\frac{\partial c_d}{\partial x} = f(c_b)\left(Da_t - Da_s q_s(c_d)\right) \tag{3.23}$$

$$c_b = \lambda Da_s f(c_b)\, q_s(c_d), \tag{3.24}$$

at $x = 2\epsilon$, where

$$f(c_b) = 1 - c_b, \qquad q_s(c_d) = 1 + \tanh\left(\xi(c_d - 1)\right), \tag{3.25}$$

and

$$Da_t = \frac{\delta h q_t}{D c_{d,\mathrm{sat}}}, \quad Da_s = \frac{\delta h \mathcal{R}_s}{D c_{d,\mathrm{sat}}}, \quad \xi = \beta c_{d,\mathrm{sat}}, \tag{3.26}$$

$$\lambda = \frac{3}{2}\frac{1}{Pe}\frac{1}{\delta^2 Re}\frac{c_{d,\mathrm{sat}}}{c_{b,\max}}\frac{1}{2\epsilon^3(1-2\epsilon)(1-4\epsilon)}\frac{2+3\mu_b/\mu_0}{1-\mu_b/\mu_0}, \quad Re = \frac{\rho_0 h[w]}{\mu_0} \tag{3.27}$$

Here, Da_t is the Damköhler number for the creation of dissolved gas, Da_s is the Damköhler number for the separation of bubbles, ξ is the dimensionless number controlling the rate of increase of q_s, and λ is the ratio between the rate at which bubbles are created at the electrode and the timescale at that they are advected away by the flow.

Both Damköhler numbers are the ratio of the timescale of their 'reaction' to the timescale of diffusion of the dissolved gas.

3.3 Perturbative analysis

Based on the size of the industrially relevant parameter values given in Table 2 we will assume that the aspect ratio of the channel $\delta \ll 1$. We will also assume that the ratio of density and viscosity of the gas compared to water are small. Although ϵ is small, we will not exploit this in our simplification, to avoid the previously discussed issue of ensuring bubbles can move horizontally away from the electrode. Since there is a large uncertainty about the size of some parameters in the model, we pick the size of the dimensionless parameters to be such that we obtain the richest possible distinguished limit, where the maximum number of terms is obtained. This is when

$$Pe = O\left(\delta^{-2}\right), \quad Fr = O(\delta), \quad Da_t = O(1), \quad Da_s = O(1), \quad \lambda = O(1), \tag{3.28}$$

and so we write

$$\delta^2 Pe = \mathcal{P}, \quad Fr/\delta = \mathcal{F}, \tag{3.29}$$

Dimensionless Parameter	Value
ϵ	1×10^{-2}
δ	1×10^{-4}
Pe	6.87×10^{5}
Fr	2.23×10^{-3}
Da_t	2.48×10^{5}
Da_s	2.48×10^{-3}
λ	4.16×10^{10}
ξ	1
$\mathcal{P}$	6.87×10^{-3}
$\mathcal{F}$	11.21

Table 2. Dimensionless parameters for the gas transport model.

where $\mathcal{P} = O(1)$, $\mathcal{F} = O(1)$. Then, seeking an asymptotic expansion in powers of δ

$$c_b \sim c_b^{(0)} + \delta c_b^{(1)} + \cdots, \tag{3.30}$$

and similarly for c_d, we find at leading-order that the problem reduces to

$$\mathcal{P}x(1-x)\frac{\partial c_d}{\partial z} = \frac{\partial^2 c_d}{\partial^2 x^2}, \tag{3.31}$$

$$\mathcal{F}^2 x(1-x)(1-2x)\frac{\partial c_b}{\partial x} + \frac{\partial c_b}{\partial z} = 0, \tag{3.32}$$

for $2\epsilon < x < 1 - 2\epsilon$, $0 < z < 1$. These governing equations are identical to the full problem, except with vertical diffusion of the dissolved gas neglected. They are subject to the following boundary conditions

$$c_b = 0, \quad c_d = 0, \quad \text{at } z = 0, \tag{3.33}$$

$$\left.\begin{aligned} -\frac{\partial c_d}{\partial x} &= f(c_b)\left(Da_t - Da_s q_s(c_d)\right) \\ c_b &= \lambda Da_s f(c_b)\, q_s(c_d), \end{aligned}\right\} \quad \text{at } x = 2\epsilon, \tag{3.34}$$

$$c_b = 0, \quad \frac{\partial c_d}{\partial x} = 0, \quad \text{at } x = 1 - 2\epsilon. \tag{3.35}$$

Note that we do not include the boundary condition at $z = 1$, (3.22), since neglecting vertical diffusion lowers the order of the dissolved gas equation in the z-direction, leaving us unable to satisfy it. Incorporating this boundary condition would require considering a boundary layer near $z = 1$, but as we except this to have little effect on the upstream solution, we do not pursue this further.

Parameter	Symbol	Value
Reduced Péclet number	$\mathcal{P}$	250 – 2000
Damköhler number (dissolved gas)	Da_t	25
Bubble radius to channel width ratio	ϵ	0
Mesh size (x-direction)	Δx	0.0025

Table 3. Parameters used in the no-bubble problem in §3.4

3.4 No bubble solution and numerical strategies

We briefly consider the behaviour when no bubbles are created, *i.e.* $Da_s = 0$ and $c_b = 0$. Then, the problem reduces to find c_d such that:

$$\mathcal{P}x(1-x)\frac{\partial c_d}{\partial z} = \frac{\partial^2 c_d}{\partial^2 x^2} \quad \text{in } [2\epsilon, 1-2\epsilon]\times[0,1], \tag{3.36}$$

$$c_d = 0 \quad \text{at } z = 0, \tag{3.37}$$

$$-\frac{\partial c_d}{\partial x} = Da_t \quad \text{at } x = 2\epsilon, \tag{3.38}$$

$$-\frac{\partial c_d}{\partial x} = 0 \quad \text{at } x = 1-2\epsilon. \tag{3.39}$$

To efficiently solve this problem, we consider a method of lines approach in which we step in the z variables using a well-established ODE solver. Indeed, consider a mesh of N points in the interval $[2\epsilon, 1-2\epsilon]$ which we denote by $\{x_j\}_{j=1}^N$, where $x_1 = 2\epsilon$ and $x_N = 1-2\epsilon$. Using a centred difference for the second derivative, the PDE (3.36) becomes

$$\mathcal{P}x_j(1-x_j)\frac{dc_{d,j}}{dz} = \frac{c_{d,j-1} - 2c_{d,j} + c_{d,j+1}}{(\Delta x)^2}, \quad j = 1, 2, \ldots, N, \tag{3.40}$$

where Δx is the mesh size. Here, $c_{d,j} := c_d(x_j, z)$ for $0 \le z \le 1$. In turn, the boundary conditions (3.38)-(3.39) become

$$\frac{c_{d,2} - c_{d,0}}{2\Delta x} + Da_t = 0, \tag{3.41}$$

$$\frac{c_{d,N+1} - c_{d,N-1}}{2\Delta x} = 0, \tag{3.42}$$

where $c_{d,0}$ and $c_{d,N+1}$ are standard notation for ghost nodes. The system (3.40)-(3.42) is solved using MATLAB's `ode15s`, which is a standard DAE solver. This allows us to properly handle the left-hand side of (3.40) whenever $x_j \approx 0$ or $x_j \approx 1$. Moreover, the numerical scheme can easily be extended to the case where (3.41) contains a nonlinear term depending on c_d (as it is the case in the problem *with* bubbles).

In Figure 7 we show the solution to the problem without production of bubbles for $\mathcal{P} = 500, 1000$, and 1500. It is clear that as the reduced Péclet number increases, there is less concentration of dissolved gas in the channel. Moreover, in Figure 8 we show the contours of concentration when $c_d = c_{d,sat}$, which correspond to the contours of $\hat{c}_d = 1$. The parameters used for these experiments are available in Table 3 and the code to obtain these figures is available at https://github.com/javieralmonacid/bubbles-in-flow-streams. In particular, Figures 7 and 8 can be reproduced by running the MATLAB script `RUNNER_NO_BUBBLES.m`.

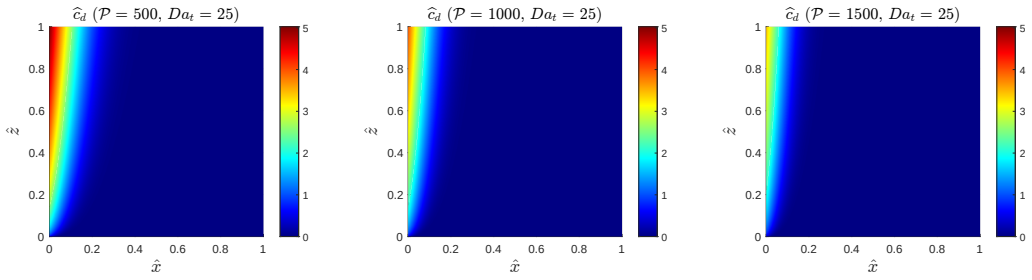

Figure 7. Concentration of dissolved gas in the absence of bubbles for different reduced Péclet numbers.

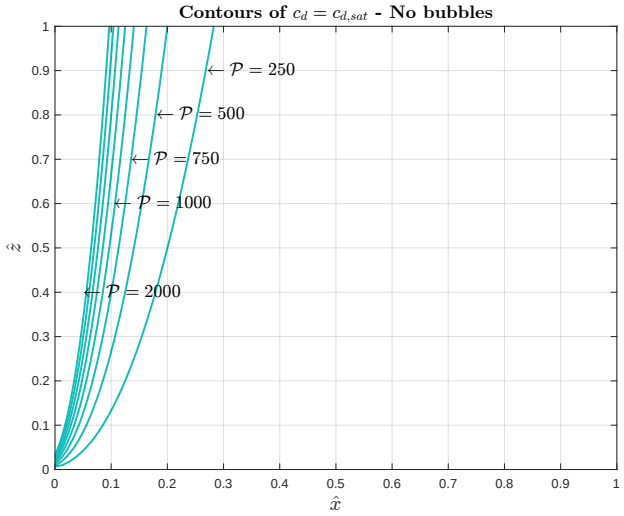

Figure 8. Contours of $c_d = c_{d,sat}$, that is $\hat{c}_d = 1$, for different reduced Péclet numbers.

3.5 Dissolved gas and bubble solutions

We now solve the coupled problem for both the dissolved gas and the bubble behaviour. We start by noting that the hyperbolic nature of the bubble equation (3.32) means it is difficult to solve numerically. Therefore, we adopt a combined analytical-numerical approach to solve the problem.

We first notice that the boundary condition for c_b in (3.34) can be rewritten as

$$c_b = \frac{\lambda Da_s q_s\left(c_d(z)\right)}{1 + \lambda Da_s q_s\left(c_d(z)\right)}, \qquad \text{at } x = 2\epsilon. \tag{3.43}$$

This, in turn, can be used to convert the other boundary condition in (3.34) into:

$$-\frac{\partial c_d}{\partial x} = \frac{Da_t - Da_s q_s(c_d)}{1 + Da_s \lambda q_s(c_d)}, \qquad \text{at } x = 2\epsilon. \tag{3.44}$$

This provides a formula for the flux of dissolved gas out of the electrode, in terms of the concentration of dissolved gas. Hence, equation (3.31), along with the boundary conditions (3.33), (3.35), and (3.44) form a closed problem for c_d only, and hence can be

solved numerically, using techniques identical to those described in §3.4 for the no bubble problem.

Once the value of c_d is known, we can evaluate (3.43), to give c_b as a function of z at $x = 2\epsilon$, which we write as

$$c_b = \Gamma(z), \qquad \text{for } x = 2\epsilon, \tag{3.45}$$

for compactness. We can then solve the remaining governing equation (3.32) for c_b, with boundary data given by (3.33), (3.35), and (3.45) using the method of characteristics. We immediately see that c_b will be constant along curves satisfying

$$\frac{\mathrm{d}x}{\mathrm{d}z} = \mathcal{F}^2 x(1-x)(2-x). \tag{3.46}$$

It is straight forward to solve this, and so find that the solution is given by

$$c_b(x,z) = \Gamma\left(z - \frac{1}{\mathcal{F}^2}\left(\log\left(\frac{x}{2\epsilon}\right) - 2\log\left(\frac{1-2x}{1-4\epsilon}\right) + \log\left(\frac{1-x}{1-2\epsilon}\right)\right)\right), \tag{3.47}$$

in the region

$$z > \frac{1}{\mathcal{F}^2}\left(\log\left(\frac{x}{2\epsilon}\right) - 2\log\left(\frac{1-2x}{1-4\epsilon}\right) + \log\left(\frac{1-x}{1-2\epsilon}\right)\right). \tag{3.48}$$

If (3.48) is not satisfied, then c_b is zero.

In Figure 9a, we plot the characteristics of the bubble equation (3.32). These show that bubbles will move towards the centreline of the channel, irrespective of where they are created. This is because the horizontal velocity of the bubble (3.5) depends on the shear rate, which goes to zero at the centre of the channel. Our model therefore predicts that bubbles will only ever occupy the half of the channel closet to the electrode. The curve seperating the bubble-containing region from the bubble-free region is shown in red. We show how this curve varies with reduced Froude number $\mathcal{F}$ in Figure 9b. This shows that increasing $\mathcal{F}$, i.e. increasing the relative size of inertial fluid forces on the bubble compared to gravity, can have a large effect on the size of the region containing bubbles. In particular, for $\mathcal{F} < 1$, the bubbles are confined to a narrow region adjacent to the electrode, while for $\mathcal{F} > 10$ they will occupy almost the entire half-channel. Variation of $\mathcal{F}$ can be achieved in practice by altering the flow speed or the channel length.

We portray the solution to the full problem (i.e. including dissolved gas and bubble concentration) in Figure 10. These have been obtained using the parameters in Table 2, which correspond to the right channel of the device in which hydrogen gas is generated. The mesh size for the numerical solution was $\Delta x = 0.0025$.

Notice that in this case, we do not observe a plume in the concentration profile of dissolved gas (Figure 10 left). This is because we have chosen a pressure gradient so that $\mathcal{F} \approx 10$. In turn, a higher pressure gradient will yield a higher reduced Péclet number. However, given that both the reduced Péclet and Froude numbers are proportional to the pressure gradient but with different constants of proportionality, we expect in this case to have an even larger reduced Froude number. This would cause a concentration profile of bubbles whose variation is too sharp to be visualized in detail in this report (this is because of the sharp curvature of the characteristics, see (3.48)). Because parameters such as the pressure gradient, the rate of generation of bubbles, the rate of generation

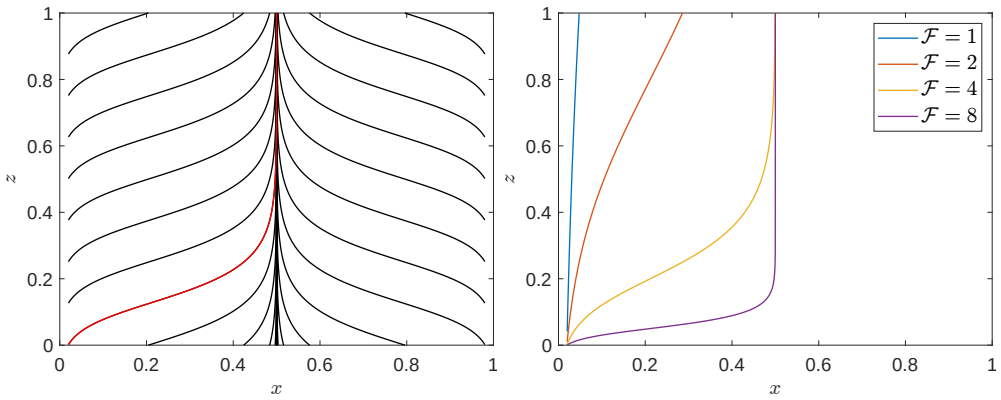

Figure 9. (left) The characteristics of (3.32) when $\mathcal{F} = 5$. The critical curve above which the bubble concentration is non-zero is shown in red. (right) The critical curve above which bubble concentration is non-zero as a function of the reduced Froude number $\mathcal{F}$.

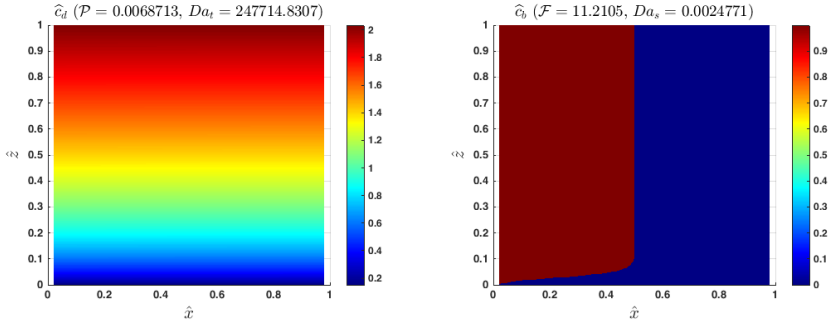

Figure 10. Full solution to the problem using the parameters in Table 2. This figure can be reproduced by running the script `RUNNER_WITH_BUBBLES.m` included in the GitHub repository.

of dissolved gas, and the bubble radius have been guessed, further research is needed to find an appropriate (and more physical) combination of parameters.

4 Discussion

In this report we have considered two simple models for gas-liquid interactions in an elecrochemical system. The first model reduces the system to an equivalent circuit, allowing us to study how the accumulation of bubbles could alter the electrical resistance at each electrode over time. The second model considers the transport of dissolved gas, and bubbles within a flowing channel adjacent to the electrode, under the simplifying assumptions that bubbles are all created at the electrode, and are of equal size, and their velocity is given by Hadamard–Rybczynski. Preliminary results are presented for both models, although there is a great deal of uncertainty about the size of the parameters related to bubble production. However, we have identified a key dimensionless parameter, the reduced Froude number $\mathcal{F}$, defined in (3.29), which controls the proportion of the

channel occupied by bubbles, and whose size can be varied purely as a function of the channel geometry.

There are many mathematical interesting and industrially-relevant directions future work on this topic could explore including:

- A fully coupled multiphase model for the gas-liquid flow in the channels around the seperator.
- Creation, merger, and evaporation of bubbles within the bulk of the flow.
- A more realistic model for formation and separation of bubbles from the separator.
- Transport of ions within the porous separator.
- Transfer of mass between the two channels via electrochemical reactions.
- Parameterision of the model through experiments.

References

[IH10] M. Ishii and T. Hibiki. *Thermo-fluid dynamics of two-phase flow*. Springer Science & Business Media, 2010.

[JM00] W. Jäger and A. Mikelić. On the interface boundary condition of Beavers, Joseph, and Saffman. *SIAM J. Appl. Math.*, 60(4):1111–1127, 2000.

[PNBT07] O. A. Petrii, R. R. Nazmutdinov, M. D. Bronshtein, and G. A. Tsirlina. Life of the Tafel equation: Current understanding and prospects for the second century. *Electrochim. Acta*, 52(11):3493–3504, 2007.

[RH23a] A. Rajora and J. W. Haverkort. An analytical model for the velocity and gas fraction profiles near gas-evolving electrodes. *Int. J. Hydrogen Energ.*, 2023.

[RH23b] A. Rajora and J. W. Haverkort. An analytical model for the velocity and gas fraction profiles near gas-evolving electrodes. *Int. J. Hydrogen Energ.*, 2023.

[SDD15] J. Schillings, O. Doche, and J. Deseure. Modeling of electrochemically generated bubbly flow under buoyancy-driven and forced convection. *Int. J. Heat Mass Tran.*, 85:292–299, 2015.

[SS21] L. M. Siqveland and S. M Skjæveland. Derivations of the Young-Laplace equation. *Capillarity*, 4(2):23–30, 2021.